Int. J. Electrochem. Sci., 15 **(2020)** 12534 – 12547, doi: 10.20964/2020.12.31

International Journal of
ELECTROCHEMICAL
SCIENCE
www.electrochemsci.org

5-(4-methoxyphenyl)-3h-1, 2-dithiole-3-thione as an Effective Inhibitor for Corrosion of Bridge Steel in Chloride media

Qiang Li[1], *Xiuli Zuo*[2], *Guicheng Yu*[3], *Jian Wang*[4,*], *Bing Sun*[4]

[1] CRCC Chongqing Investment Group CO., LTD, Chongqing 405806, China
[2] Department of Petroleum, Army Logistics University of PLA, Chongqing 401331, China
[3] Gas Storage Management Department, Petro China Southwest Oil & Gasfield Company, Chongqing 401147, China.
[4] College of Mechanical Engineering, Chongqing University, Chongqing 400044, China.
*E-mail: vi@cqu.edu.cn, wangj_cqu@163.com

Received: 3 August 2020 / *Accepted:* 20 September 2020 / *Published:* 31 October 2020

Anethole trithione (5-(4-methoxyphenyl)-3h-1, 2-dithiole-3-thione, MDT), as a green and environmentally friendly corrosion inhibitor, is studied for bridge steel (BS) in hydrochloric acid medium via electrochemical impedance spectroscopy (EIS) technology, open circuit potential (OCP) test, and potentiodynamic polarization (PDP) curve test, scanning electron microscope (SEM) test, quantum chemistry calculation (QCC) and molecular dynamics (MD) simulation. The open circuit potential indicates that the steel electrode can reach a stable state after the bridge steel is soaked in hydrochloric acid for 1200 seconds. The polarization curve data show that MDT can reduce the value of the corrosion current density, and as the temperature increases, the corrosion inhibition efficiency of MDT for bridge steel increases significantly. In addition, the adsorption isotherm model study shows that the adsorption of MDT at the surface of BS is consistent with Langmuir adsorption. Both QCC and MD show that MDT can be adsorbed at the surface of bridge steel in parallel way to obtain the largest coverage area.

Keywords: MDT; corrosion inhibitor; EIS; molecular dynamics simulation; SEM; Langmuir single-layer adsorption

1. INTRODUCTION

The problem of metal corrosion protection has always been a hot area for corrosion workers to explore. Significant economic losses globally due to metal corrosion [1]. From a certain perspective, the problem of metal corrosion is a huge obstacle to the progress of human civilization. Therefore, in recent years, corrosion scientists have developed a large number of corrosion protection methods. Among them,

the use of corrosion inhibitors is one of the most commonly used and effective methods. Therefore, the corrosion inhibitor has been recognized and loved by vast corrosion scientists.

Corrosion inhibitors usually have their own unique properties, such as sulfur, oxygen, nitrogen, phosphorus or some unsaturated functional groups, etc [2-7]. These unique characteristics allow the organic inhibitor to give lone electrons and empty orbitals of the metal to form coordination bonds, which can be firmly adsorbed on the metal surface, thereby effectively inhibiting the corrosion of the metal. In recent years, a lot of corrosion scientists have studied different types of green corrosion inhibitors. These green corrosion inhibitors include amino acids, natural plant extracts, edible flavors, and various oral drugs. Among them, the research on oral corrosion inhibitors deserves more attention from corrosion scientists. First of all, oral drugs have their own expiration date. If they exceed the expiration date, they cannot be taken by people. Therefore, the use of expired oral drugs as corrosion inhibitors can maximize the use of resources and avoid waste of resources. On the other hand, since oral administration can be directly eaten by the human body, it has very little impact on the environment in the case of small doses. In this paper, we studied MDT as a green inhibitor. MDT is an efficient cholecystitis drug, which can be directly absorbed by the body. Therefore. MDT as a corrosion inhibitor has negligible impact on the ecological environment.

We used different electrochemical ways and theoretical calculations tool to insight into the corrosion inhibition behavior of MDT on bridge steel, respectively. Both results show that MDT can effectively inhibit the corrosion of bridge steel in hydrochloric acid.

2. EXPERIMENTAL

2.1 Materials

5-(4-methoxyphenyl)-3h-1, 2-dithiole-3-thione (MDT) was purchased from Guojia Pharmaceutical Company, its molecular structure is shown in Figure 1. The chemical composition of bridge steel (BS) is Mn 1.6%, Si 0.17%, Cr 0.16%, C 0.06%, Nb 0.04%, Al 0.035% and the remaining Fe. BS are cut into 1×1×1 cm and 0.5×0.5×0.5 cm samples to make working electrodes and SEM test. MDT is formulated into 10, 20, 40, 80 mg/L test solution in 1 M hydrochloric acid solution. BS samples are immersed in hydrochloric acid for two hours and then subjected to SEM morphology.

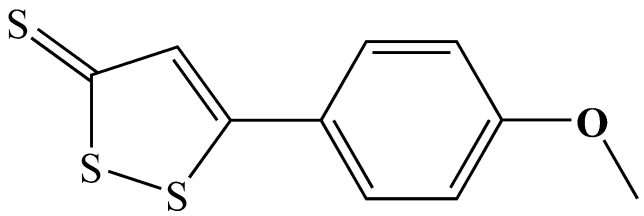

Figure 1. The molecular structure of MDT.

2.2. Electrochemical tests

The electrochemical experiment of this work was carried out in the Shanghai Chenhua electrochemical workstation (China, CHI760E) via a three-electrode cell at 298 K, 308 K, and 318 K. In this three-electrode system, BS is used as the working electrode, Pt is used as the counter electrode, and the saturated calomel electrode is used as the auxiliary electrode. When the open circuit potential test is performed, the time of the OCP test is 1200 seconds to ensure that the BS surface obtains a stable condition. The EIS test is carried out on the basis of a stable open circuit potential, and the test frequency range is 100000 Hz to 0.01 Hz. The range of the PDP curve is from E_{OCP}+250 mV to E_{OCP}−250 mV. The rate of polarization is 2 mV/s. The formulas for calculating the corrosion inhibition efficiency are as follows [8-17]:

$$\eta(\%) = \frac{R_{ct} - R_{ct,0}}{R_{ct}} \times 100 \quad (1)$$

$$\eta(\%) = \frac{i_{corr,0} - i_{corr}}{i_{corr,0}} \times 100 \quad (2)$$

2.3. Theoretical calculation details

The quantum chemical parameters of MDT are calculated using Material Studio software. Structural optimization as a calculation task, force field chooses COMPASS, and Calculate the basis set as DNP. The adsorption model of MDT on Fe (110) surface is calculated using the Forceite module in MS software. Fill the 3D Fe model (7×7×7) with one MDT molecule and 100 water molecules. NVT as the Ensemble. Total simulation time is 700 ps, and Time step is 1fs.

3. RESULTS AND DISCUSSION

3.1 Corrosion effect of temperature for BS in HCl medium

Figure 2 (a) and (b) show the Nyquist and Bode diagrams of BS soaked in 1M hydrochloric acid without MDT, respectively. As shown in Figure 2(a), the semi-diameter of the capacitive loop arc decreases significantly with the increase of temperature. And when the temperature is 318 K, the arc semi-diameter of the capacitive loop decreases significantly faster than 308 K, so it can be proved that the temperature increase will accelerate the corrosion of BS in the hydrochloric acid solution [18]. Table 1 is the EIS data obtained by fitting the equivalent circuit diagram. It can be found that when the temperature is 298 K, the charge transfer resistance at this time is 48.7 Ω cm^2. When the temperature rises to 308 K and 318 K, the charge transfer resistance on the BS surface is 40.4 Ω cm^2 and 26.4 Ω cm^2. Therefore, it can be strongly proved that temperature increase will accelerate the corrosion of BS in hydrochloric acid medium [19-21]. Figure 2 (b) is the corresponding Bode diagram. As the temperature increases, the phase angle diagram and the impedance modulus diagram become narrower and lower, which indicates that the temperature increase will accelerate the corrosion of BS. Therefore, it can be proved that as the temperature increases, the corrosion of metals in the corrosive medium will increase significantly [22, 23].

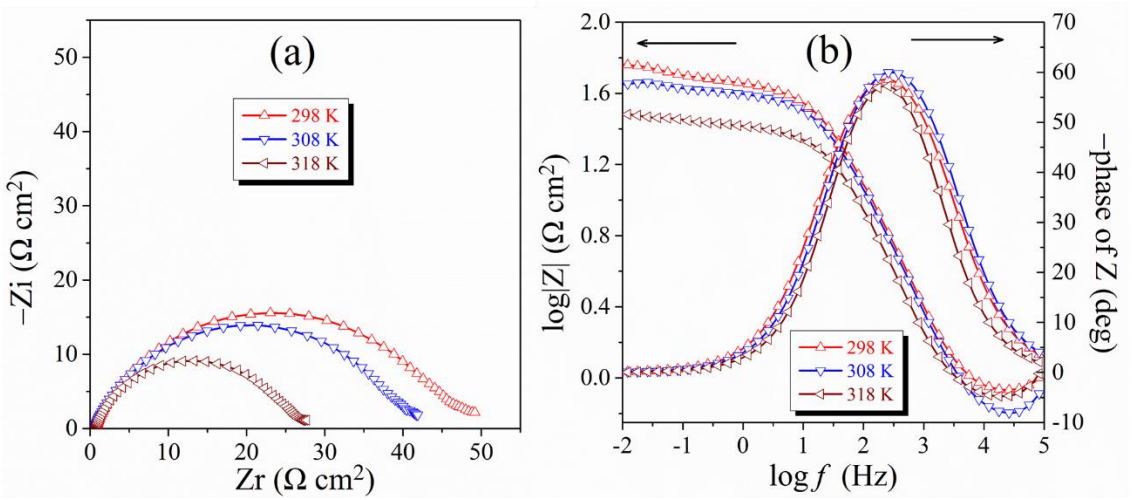

Figure 2. (a) and (b) show the Nyquist and Bode diagrams of BS soaked in 1 M hydrochloric acid without MDT at 298 K, 308 K, and 318 K, respectively.

Figure 3 (a) and (b) show the potentiodynamic polarization curve and open circuit potential diagram of BS steel under blank solution conditions at 298 K, 308 K, and 318 K, respectively. As shown in Figure 3 (b), the open circuit potential becomes stable after 1200 seconds, and the OCP curve tends to move to the cathode. This indicates that the increase in temperature will accelerate the evolution of hydrogen [22, 23]. In addition, in Figure 3(a), as the temperature increases from 298 K to 318 K, the corrosion current density increases from 37.3 mA cm^{-2} to 68.9 mA cm^{-2}. Therefore, it can be judged by the change of corrosion current density that increasing the temperature will accelerate the corrosion of BS in hydrochloric acid.

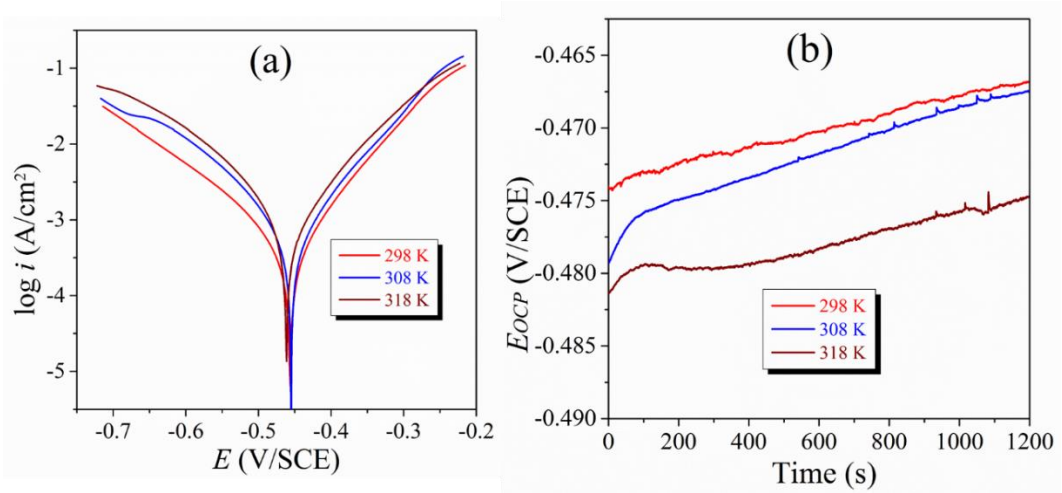

Figure 3. (a) and (b) show the potentiodynamic polarization curve and open circuit potential diagram of BS steel under blank solution conditions at 298 K, 308 K, and 318 K, respectively.

Figure 4 (a) and (b) show Nyquist and Bode diagrams of BS immersed in 1 M hydrochloric acid solution containing 80 mg/L MDT at 298 K, 308 K, and 318 K, respectively. In Figure 4 (a), after adding

80 mg/L of MDT. The semi-diameter value of the capacitive loop arc increased markedly, and the charge transfer resistance values at 298 K, 308 K and 318 K were 247.8 Ω cm^2, 221.1 Ω cm^2 and 170.1 Ω cm^2, respectively. The corrosion inhibition efficiency values calculated by formula 1 are 80.3%, 81.7% and 84.5%, respectively. Therefore, it can be judged that as the temperature increases, MDT can show better corrosion inhibition performance. This may be because the adsorption of MDT on the surface of BS is relatively tight and not easy to fall off [18]. The impedance modulus diagram and phase angle diagram in Figure 4 (b) are significantly higher and wider than the blank solution, which shows that MDT can exhibit good corrosion inhibition performance [24, 25].

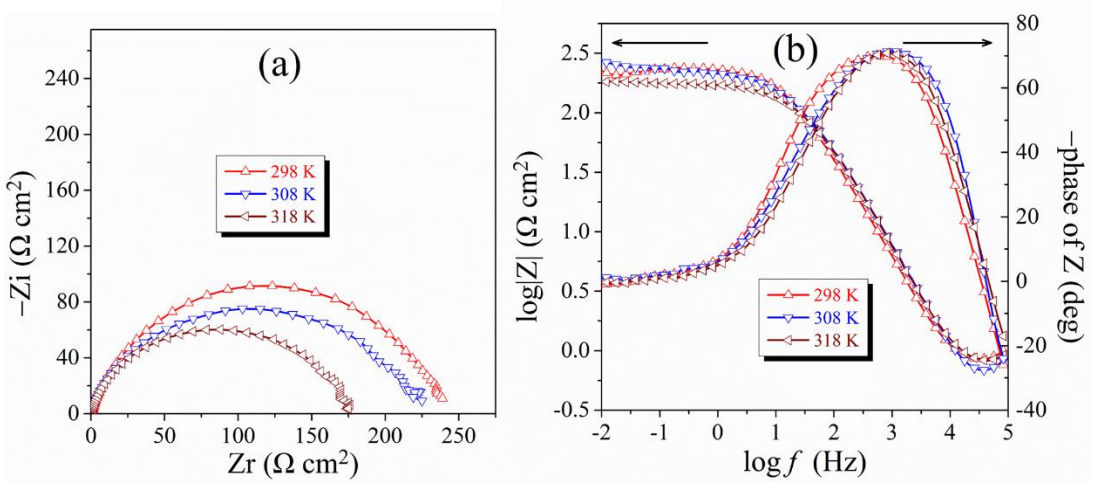

Figure 4. (a) and (b) show Nyquist and Bode diagrams of BS immersed in 1 mol/L hydrochloric acid containing 80 mg/L MDT at 298 K, 308 K, and 318 K, respectively.

Figure 5 (a) and (b) show potentiodynamic polarization curve and open circuit potential diagram of BS immersed in 1 mol/L HCl containing 80 mg/L MDT at 298 K, 308 K, and 318 K, respectively. As shown in Figure 5 (a), after adding 80 mg/L MDT to the hydrochloric acid solution, the value of the corrosion current density is significantly lower than that of the blank solution. As shown in Table 2, the corrosion current density at 298 K dropped from 37.3 mA cm^{-2} in the blank solution to 6.4 mA cm^{-2}. At 308 K, the corrosion current density dropped from 48.2 mA cm^{-2} in the blank solution to 7.7 mA cm^{-2}. At 318 K, the corrosion current density dropped from 68.9 mA cm^{-2} in the blank solution to 9.3 mA cm^{-2}. The corresponding corrosion inhibition efficiencies calculated by formula 2 are 82.8%, 84.1%, and 86.5%, respectively. Therefore, this is consistent with the results obtained by EIS. Increasing the temperature within a certain range MDT can show better corrosion inhibition efficiency. Figure 5(b) is the corresponding open circuit potential curve, it can be found that after 1200 seconds, it is obviously stable. It is also worth mentioning that the change value of the corrosion potential is significantly less than 85 mV, so it can be judged that MDT is a mixed corrosion inhibitor [26].

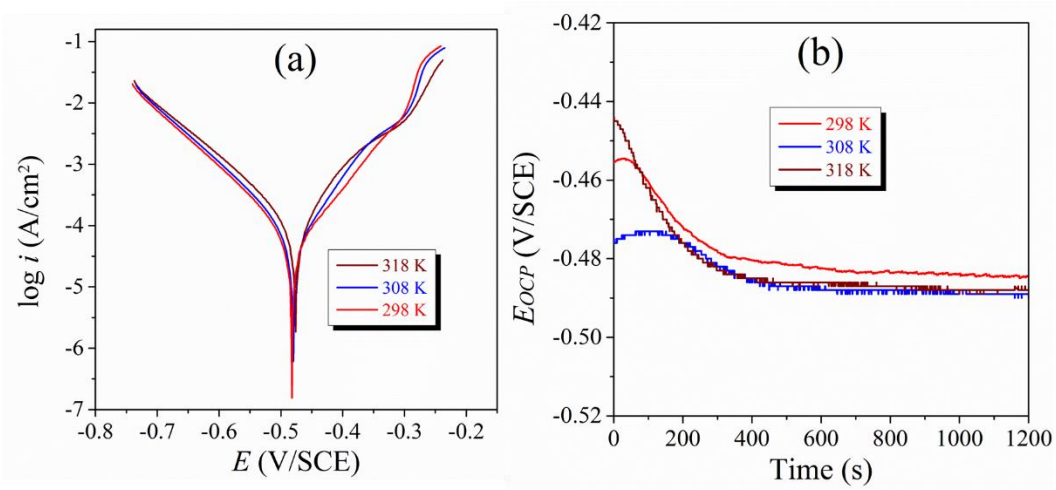

Figure 5. (a) and (b) show potentiodynamic polarization curve and open circuit potential diagram of BS immersed in 1 mol/L hydrochloric acid medium containing 80 mg/L MDT at 298 K, 308 K, and 318 K, respectively.

Table 1. EIS fitted data with and without MDT at different temperatures.

T (K)	C (mg/L)	R_s (Ω cm^2)	$Y_0\times10^{-6}$ (S s^n cm^{-2})	n	C_{dl} (μF cm^{-2})	R_{ct} (Ω cm^2)	η (%)
298	0	0.87	429.9	0.80	123.7	48.7	-
	80	0.90	65.9	0.88	61.8	247.8	80.3
308	0	0.69	440.1	0.82	135.3	40.4	-
	80	0.72	73.7	0.87	74.4	221.1	81.7
318	0	0.86	461.8	0.85	144.6	26.4	-
	80	0.83	88.5	0.88	88.9	170.1	84.5

Table 2. The polarization curve data of BS immersed in 1M hydrochloric acid solution at different temperatures.

T (K)	C (mg/L)	E_{corr} (V/SCE)	i_{corr} (mA cm^{-2})	β_c (mV dec^{-1})	β_a (mV dec^{-1})	η (%)
298	0	–0.456	37.3	–123	86	—
	80	–0.480	6.4	-102	73	82.8
308	0	–0.455	48.2	–111	92	—
	80	–0.482	7.7	–102	78	84.1
318	0	–0.461	68.9	–114	91	—
	80	–0.476	9.3	–107	101	86.5

3.2 Influence of concentration on the anti-corrosion nature of MDT

Figure 6 (a) and (b) show Nyquist and Bode diagrams at 298 K when BS is immersed in 1 mol/L hydrochloric acid medium with different concentrations MDT, respectively. In Figure 6 (a), as the MDT concentration increases, the capacitive loop arc radius shows an increasing trend. According to the fitting of the equivalent circuit diagram in Figure 8, when the concentration is 10 mg/L, 20 mg/L, 40 mg/L, and 80 mg/L, the corresponding charge transfer resistance is 160.7 Ω cm^2, 181.6 Ω cm^2, 209.4 Ω cm^2, and 247.8 Ω cm^2, respectively. The corresponding corrosion inhibition efficiencies at different concentrations were 69.7%, 73.1%, 76.7%, and 80.3%, respectively. Therefore, it can be judged that as the concentration of MDT increases, the molecular protective film formed on the surface of the BS becomes more dense and orderly, so that MDT can exhibit better corrosion inhibition properties. In Figure 6 (b), with the increase of MDT concentration, the impedance modulus value is significantly increased by 1 to 2 orders of magnitude compared with the blank solution, and the phase angle diagram is also significantly wider, which indicates that MDT is an excellent inhibitor [27-29].

In addition, it is worth mentioning in Table 3 that as the concentration of MDT increases, the capacitance of the electric double layer obviously shows a decreasing trend. This experimental phenomenon can be explained by the formula (3) [23, 30, 31]:

$$C_{dl} = \frac{\varepsilon^0 \varepsilon}{d} S \quad (3)$$

where S is the BS area. The d is C_{dl} thickness. According to formula 3, it can be concluded that the more water molecules on the surface of the BS steel substituted by MDT, the better the MDT can exhibit good corrosion inhibition performance.

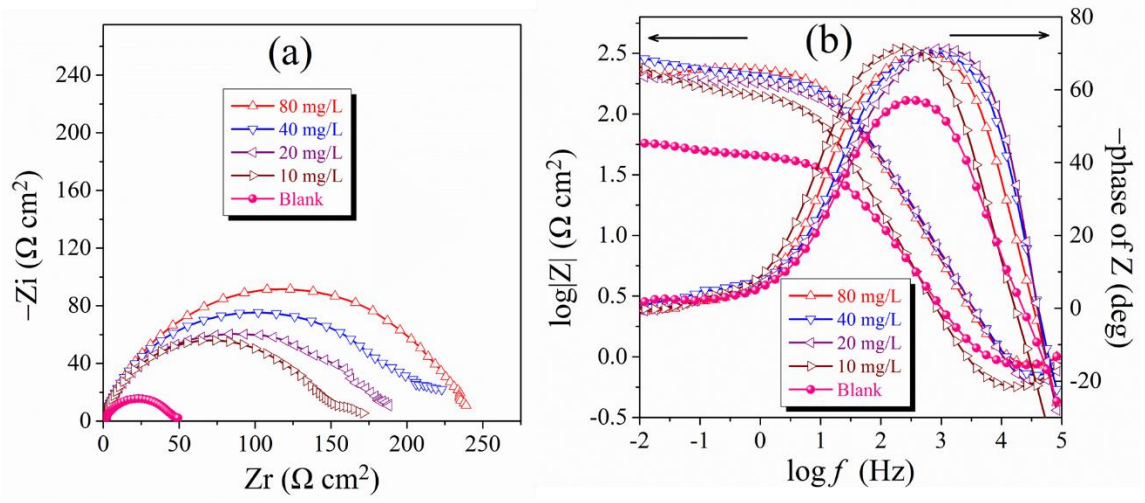

Figure 6 (a) and (b) show Nyquist and Bode diagrams at 298 K when BS is immersed in 1 mol/L hydrochloric acid medium without and with different concentrations MDT.

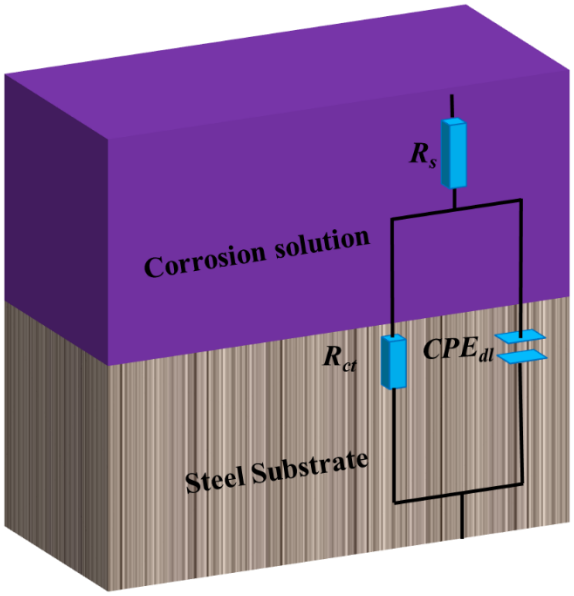

Figure 7. Equivalent circuit graph for fitting EIS data.

Table 3. Impedance spectroscopy parameters at different concentrations MDT.

C (mg/L)	R_s (Ω cm^2)	$Y_0\times10^{-6}$ (S s^n cm^{-2})	n	C_{dl} (μF cm^{-2})	R_{ct} (Ω cm^2)	η (%)
Blank	0.87	429.9	0.80	123.7	48.7	-
MDT						
10	0.69	188.0	0.90	86.3	160.7	69.7
20	0.66	74.5	0.87	75.5	181.6	73.1
40	0.73	71.3	0.86	66.2	209.4	76.7
80	0.90	65.9	0.88	61.8	247.8	80.3

Figure 8 (a) and (b) show potentiodynamic polarization curve and open circuit potential diagram of BS immersed in 1 mol/L hydrochloric acid medium containing different concentration MDT at 298 K, respectively. It can be clearly found that with the increase of MDT concentration, both the anode and cathode branches of the polarization curve have a decreasing trend, which shows that DMT can effectively inhibit the iron dissolution of the anode and the cathode hydrogen evolution. In addition, the curves of the all cathodic branches show the parallel trend, which indicates that DMT does not change its reaction mechanism after adsorption on the BS surface [25, 26, 32-35]. Besides, it can be found from Table 4 that after adding DMT, the change in corrosion potential is significantly less than 85 mV, so it can be judged that DMT is a mixed inhibitor [22, 36]. When the concentration is 80 mg/L, the η is 82.8%. Figure 8 (b) is the corresponding OCP diagram. It can be found that after adding DMT, the OCP curve generally shifts to the anode direction, which shows that MDT can effectively inhibit the precipitation of anode iron ions.

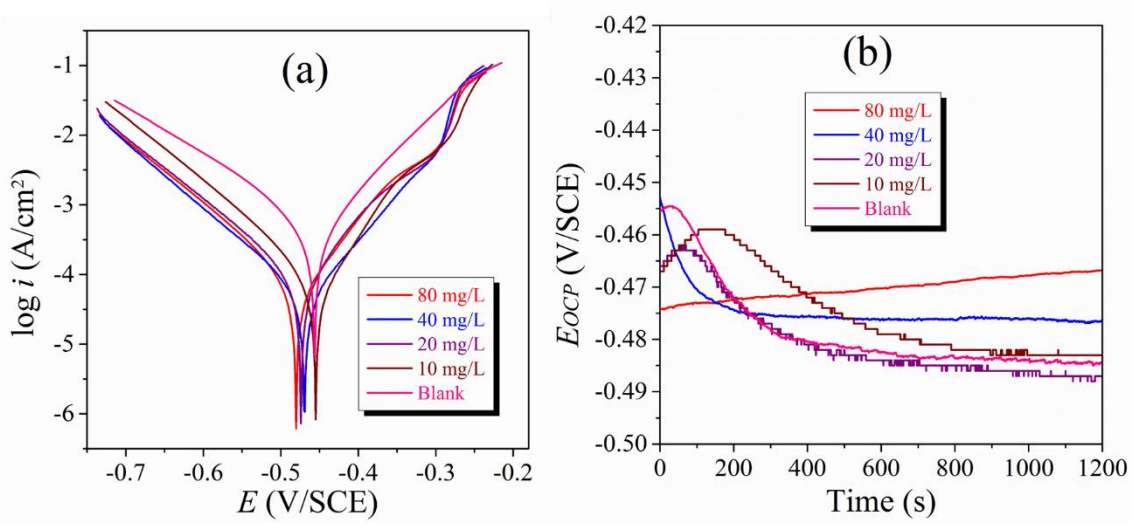

Figure 8. (a) and (b) show potentiodynamic polarization curve and open circuit potential diagram of BS immersed in 1 mol/L hydrochloric acid medium with and without different concentration MDT at 298 K.

Table 4. Polarization curve parameters at different MDT concentrations.

C (mg/L)	E_{corr} (V/SCE)	i_{corr} (mA cm^{-2})	β_c (mV dec^{-1})	β_a (mV dec^{-1})	η (%)
Blank	–0.456	37.3	–123	85	—
MDT					
10	–0.455	10.7	–99	67	71.3
20	–0.474	9.0	–107	91	75.8
40	–0.469	7.9	–108	75	78.7
80	–0.480	6.4	–103	73	82.8

3.3 Adsorption isotherm model research

In order to further understand the adsorption information of MDT on the BS surface, we used different adsorption isotherms to study the adsorption behavior of MDT on the surface of BS. The fitting results show that the adsorption of MDT on the BS surface conforms to the Langmuir mono-layer adsorption. The expression is as follow [20, 37-40]:

$$\frac{C}{\theta} = \frac{1}{K_{ads}} + C \qquad (4)$$

The fitted experimental results are listed in Table 9, where K_{ads} is the adsorption equilibrium constant, and the adsorption equilibrium constant of MDT onto the surface of BS is 358.4 L/g. This large adsorption equilibrium constant manifests that MDT can be closely adsorbed on the surface of BS [34]. In addition, in order to judge the adsorption type of MDT on the BS surface, we calculated the value of ΔG^0_{ads} using the following formula [18, 33, 41]:

$$K_{ads} = \frac{1}{1000}\exp(-\frac{\Delta G^0_{ads}}{RT}) \qquad (5)$$

The calculated ΔG_{ads}^{0} value is –31.7 kJ/mol, which indicates that MDT has both physical and chemical adsorption on the BS surface [32].

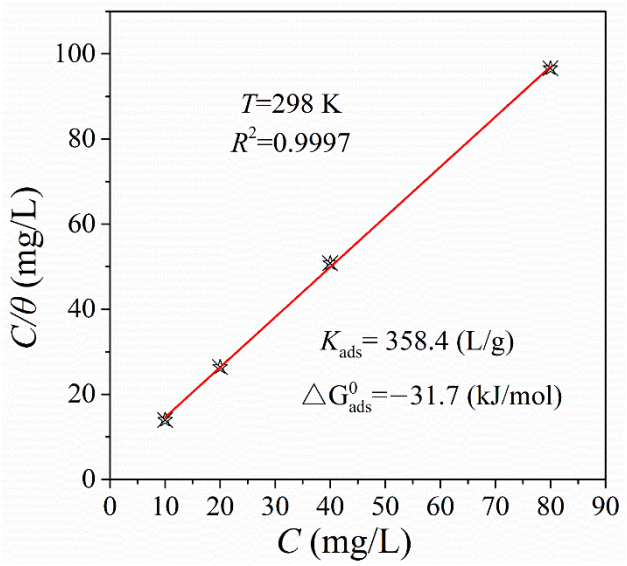

Figure 9. Langmuir isotherm adsorption for BS immersed in 1 M HCl medium with different MDT at 298 K.

3.4 SEM surface topography analysis

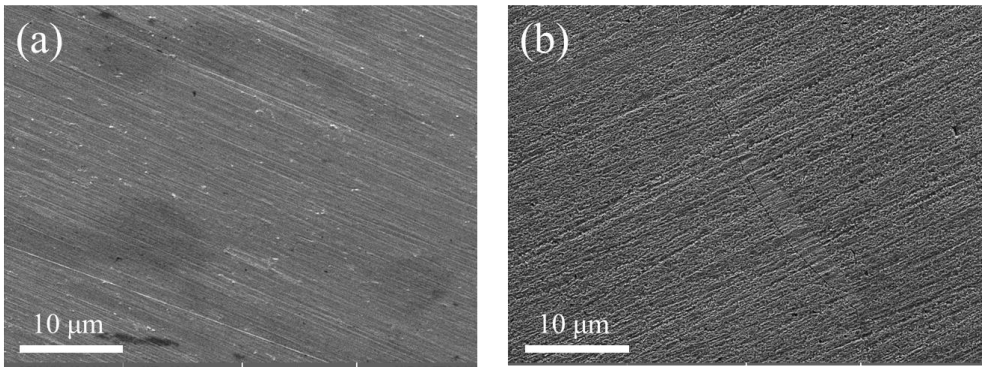

Figure 10. (a) and (b) show the surface topography of BS immersed in 1 mol/L hydrochloric acid solution for 1 hour with 80 mg/L MDT and without MDT at the 298 K, respectively.

Figure 10 (a) and (b) show the surface topography of BS steel immersed in 1 mol/L hydrochloric acid solution for 1 hour with 80 mg/L MDT and without MDT at the 298 K， respectively. In Figure 10 (a), it can be clearly found that the surface of the BS steel after adding 80 mg/L of MDT is obviously smooth and bright, and the scratches left by sandpaper polishing are faintly visible. In Figure 10 (b), there are a mass of corrosion holes on the entire BS surface. These corrosion holes are relatively uniform, which indicates that uniform corrosion has occurred on the entire BS surface. By comparing Figure 10

(a) and (b), it can be found that MDT can effectively inhibit the corrosion of BS, which is consistent with the results of electrochemical experiments.

3.5 Quantum chemical analysis

Figure 11 presents the optimized molecular configuration of MDT and the electron cloud distribution of LUMO and HOMO orbitals. We can find that the optimized molecules of MDT are basically in a plane, which indicates that MDT molecules are more likely to be adsorbed in parallel on the surface of BS to obtain higher coverage. The HOMO electron cloud of MDT molecules is mainly distributed on sulfur and oxygen atoms, which manifests that these active sites to give electrons to iron atoms to form coordination bonds [42]. The LUMO orbital of MDT molecule is almost evenly distributed on the entire molecule. The LUMO orbital is the electron-acquiring ability of the MDT, so MDT molecule easily form feedback bonds with iron atoms [26]. In addition, it is worth mentioning that the dipole moment value of the MDT molecule is 5.64 D. According to many references report, inhibitor with a large dipole moment are more likely to exhibit high corrosion inhibition performance.

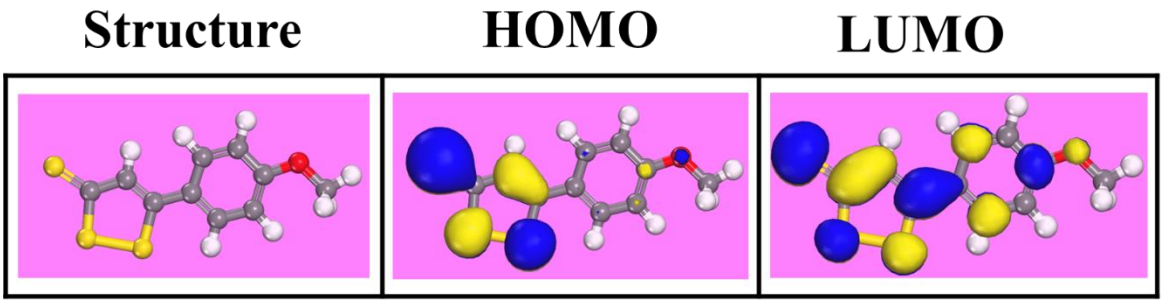

Figure 11. MDT optimized configuration and HOMO and LUMO diagrams.

3.6 Molecular dynamics simulation

Figure 12 (a) and (b) present a side view and a top view after stable adsorption of MDT on the Fe (110) surface, respectively. It can be clearly found that the adsorption of MDT on the BS surface is almost in parallel mode, which is accord with the prediction of the previous quantum chemistry calculation results. In order to further explore the adsorption energy of MDT on Fe (110) surface, we use the following formulas (6) and (7) to calculate [19, 43]:

$$E_{\text{int}\,eract} = E_{tot} - (E_{subs} + E_{inh}) \quad (6)$$

$$E_{binding} = -E_{\text{int}\,eract} \quad (7)$$

where $E_{binding}$ is the binding energy of MDT and Fe (110), E_{tot} is the total energy of the MDT, all water molecules and Fe (110), E_{subs} is the energy of the all water molecules and Fe (110), E_{inh} is refer to the MDT energy. The values of binding energy of MDT on the surface of Fe (110) are 612.8 kJ/mol. The large binding energy indicates that MDT can form a stable adsorption film on Fe (110).

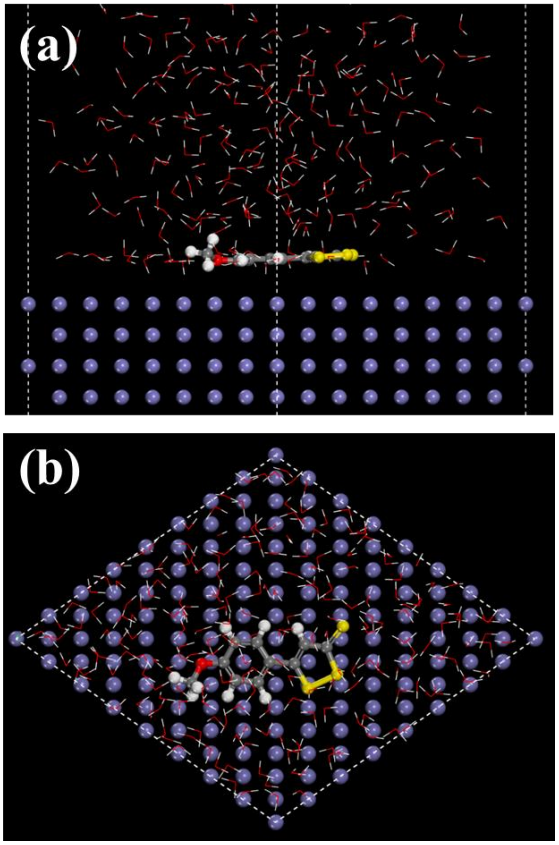

Figure 12. (a) and (b) present the side view and a top view after stable adsorption of MDT on the Fe (110) surface.

4. CONCLUSION

Electrochemical experiment data show that MDT can exhibit good anti-corrosion performance to BS, and the corrosion inhibition performance of MDT increases observably with the increase of temperature within a certain range. SEM surface topography analysis strongly proves that MDT can exhibit good corrosion inhibition performance. The adsorption of MDT onto the BS surface conforms to Langmuir single-layer adsorption. Quantum chemistry and molecular dynamics simulations have proved that MDT is an excellent corrosion inhibitor for BS in hydrochloric acid medium.

References

1. Y. Qiang, H. Li, and X. Lan, *J. Mater. Sci. Technol.*, 52 (2020) 63.
2. B. Tan, S. Zhang, Y. Qiang, L. Feng, C. Liao, Y. Xu, and S. Chen, *J. Mol. Liq.*, 248 (2017) 902.
3. M. M. Antonijevic and M. B. Petrovic, *Int. J. Electrochem. Sci.*, 3 (2008) 1.
4. M.M. Antonijević, S.M. Milić and M.B. Petrović, *Corros. Sci.*, 51 (2009) 1228.
5. J. Liu, Y. Zhou, C. Zhou and H. Lu, *Int. J. Electrochem. Sci.*, 15 (2020) 2499.
6. S. Chen, B. Zhu, and X. Liang, *Int. J. Electrochem. Sci.*, 15 (2020) 1

7. S. Y. Al-Nami, *Int. J. Electrochem. Sci*., 14 (2019) 3986.
8. M.B. Radovanović, and M.M. Antonijević, *J. Adhesion Sci. Technol*., 31 (2016) 369.
9. M.B. Petrović Mihajlović, M.B. Radovanović, Ž.Z. Tasić, and M.M. Antonijević, *J. Mol. Liq*., 225 (2017) 127.
10. Ž.Z. Tasić, M.B. Petrović Mihajlović, M.B. Radovanović, A.T. Simonović, and M.M. Antonijević, *J. Mol. Struct*., 1159 (2018) 46.
11. Ž.Z. Tasić, M.B. Petrović Mihajlović, M.B. Radovanović, and M.M. Antonijević, *J. Mol. Liq*., 265 (2018) 687.
12. J. Zhang, *Int. J. Electrochem. Sci*., 15 (2020) 1437.
13. S. Xu, W. Li, X. Zuo, D. Zheng, X. Zheng, and S. Zhang, *Int. J. Electrochem. Sci*., 14 (2019) 5777.
14. X. Wang, H. Jiang, D. Zhang, L. Hou, and W. Zhou, *Int. J. Electrochem. Sci*., 14 (2019) 1178.
15. C. Wang, W. Gou, C. Liu, D. Fu, L. Zhou, C. Lai, B. Xie, and S. Zhu, *Int. J. Electrochem. Sci*., 14 (2019) 3443.
16. A. S. Fouda, M.M. Hegazi, and A. El-Azaly, *Int. J. Electrochem. Sci*., 14 (2019) 4668.
17. M.n. Corrales-Luna, and M.T. Le, E.M. Arce-Estrada, *Int. J. Electrochem. Sci*., 14 (2019) 4420.
18. J. Zhang, L. Zhang, and G. Tao, *J. Mol. Liq*., 272 (2018) 369.
19. W. Luo, W. Li, J. Tan, J. Liu, B. Tan, X. Zuo, Z. Wang, and X. Zhang, *J. Mol. Liq*., 314 (2020) 113630.
20. L. Guo, R. Zhang, B. Tan, W. Li, H. Liu, and S. Wu, *J. Mol. Liq*., 310 (2020) 113239.
21. L. Guo, B. Tan, X. Zuo, W. Li, S. Leng, and X. Zheng, *J. Mol. Liq*., 317 (2020) 113915.
22. S. Chen, H. Zhao, S. Chen, P. Wen, and H. Wang, W. Li, *J. Mol. Liq*., 312 (2020) 113433.
23. S. Chen, S. Chen, B. Zhu, C. Huang, and W. Li, *J. Mol. Liq*., 311 (2020) 113312.
24. Y. Qiang, L. Guo, H. Li, and X. Lan, *Chem. Eng. J*., 406 (2021).
25. B. Tan, B. Xiang, S. Zhang, Y. Qiang, L. Xu, S. Chen, and J. He, *J. Colloid Interf. Sci*., 582 (2020) 918.
26. T. Yan, S. Zhang, L. Feng, Y. Qiang, L. Lu, D. Fu, Y. Wen, J. Chen, W. Li, and B. Tan, *J. Taiwan Inst. Chem. Eng*., 106 (2020) 118.
27. Y. Qiang, S. Zhang, L. Guo, X. Zheng, B. Xiang, and S. Chen, *Corros. Sci*., 119 (2017) 68.
28. Y. Qiang, S. Zhang, S. Yan, X. Zou, and S. Chen, *Corros. Sci*., 126 (2017) 295.
29. Y. Qiang, S. Zhang, L. Guo, S. Xu, L. Feng, I.B. Obot, and S. Chen, *J. Clean. Prod*., 152 (2017) 17.
30. B. Tan, S. Zhang, W. Li, X. Zuo, Y. Qiang, L. Xu, J. Hao, and S. Chen, *J. Ind. Eng. Chem*., 77 (2019) 449.
31. S. Tao, and H. Huang, *Int. J. Electrochem. Sci*., 14 (2019) 5435.
32. B. Tan, S. Zhang, Y. Qiang, W. Li, H. Li, L. Feng, L. Guo, C. Xu, S. Chen, and G. Zhang, *J. Mol. Liq*., 298 (2020) 111975.
33. B. Tan, S. Zhang, Y. Qiang, W. Li, H. Liu, C. Xu, and S. Chen, *J. Mol. Liq*., 286 (2019) 110891.
34. B. Tan, S. Zhang, H. Liu, Y. Qiang, W. Li, L. Guo, and S. Chen, *J. Taiwan Inst. Chem. E*., 102 (2019) 424.
35. Zahra Sanaei, Mohammad Ramezanzadeh, Ghasem Bahlakeh, B. Ramezanzadeh, *J. Ind. Eng. Chem*., 69 (2019) 18.
36. B. Tan, S. Zhang, Y. Qiang, L. Guo, L. Feng, C. Liao, Y. Xu, and S. Chen, *J. Colloid Interf. Sci*., 526 (2018) 268.
37. B. Tan, S. Zhang, H. Liu, Y. Guo, Y. Qiang, W. Li, L. Guo, C. Xu, and S. Chen, *J. Colloid Interf. Sci*., 538 (2019) 519.
38. Z.Z. Tasic, M.M. Antonijevic, M.B. Petrovic Mihajlovic, and M.B. Radovanovic, *J. Mol. Liq*., 219 (2016) 463.
39. X. Zhang, and B. Tan, *Int. J. Electrochem. Sci*., 13 (2018) 11388.
40. L. Gao, S. Peng, X. Huang, and Z. Gong, *Appl. Surf. Sci*., 511 (2020) 145446.
41. H. M. Elabbasy, *Int. J. Electrochem. Sci*., 14 (2019) 5355.

42. Y. Qiang, S. Zhang, and L. Wang, *Appl. Surf. Sci*., 492 (2019) 228.
43. Y. Qiang, S. Zhang, H. Zhao, B. Tan, and L. Wang, *Corros. Sci*., 161 (2019) 108193